Person identification technique using human iris recognition

Christel-loïc TISSE[1], Lionel MARTIN[1], Lionel TORRES [2], Michel ROBERT [2]

[1] Advanced System Technology
STMicroelectronics – ZI Rousset – 13106 Rousset Cedex, France
[2] Université de Montpellier, UMR 5506, L.I.R.M.M.
161, rue Ada – 34392 Montpellier, France
christel-loic.tisse@st.com, lionel.martin@st.com, torres@lirmm.fr, robert@lirmm.fr

Abstract

The biometric person authentication technique based on the pattern of the human iris is well suited to be applied to any access control system requiring a high level of security. This paper examines a new iris recognition system that implements (i) gradient decomposed Hough transform / integro-differential operators combination for iris localization and (ii) the "analytic image" concept (2D Hilbert transform) to extract pertinent information from iris texture. All these image-processing algorithms have been validated on noised real iris images database. The proposed innovative technique is computationally effective as well as reliable in terms of recognition rates.

1. Introduction

1.1 Overview

Today, biometric recognition is a common and reliable way to authenticate the identity of a living person based on physiological or behavioral characteristics. A physiological characteristic is relatively stable physical characteristics, such as fingerprint, iris pattern, facial feature, hand silhouette, etc. This kind of measurement is basically unchanging and unalterable without significant duress. A behavioral characteristic is more a reflection of an individual's psychological makeup as signature, speech pattern, or how one types at a keyboard. The degree of intra-personal variation in a physical characteristic is smaller than a behavioral characteristic. For examples, a signature is influenced by both controllable actions and less psychological factors, and speech pattern is influenced by current emotional state, whereas fingerprint template is independent. Nevertheless all physiology-based biometrics don't offer satisfactory recognition rates (false acceptance and/or false reject rates, respectively referenced as FAR and FRR). The automated personal identity authentication systems based on iris recognition are reputed to be the most reliable among all biometric methods: we consider that the probability of finding two people with identical iris pattern is almost zero [1]. That's why iris recognition technology is becoming an important biometric solution for people identification in access control as networked access to computer application [2].

Compared to fingerprint, iris is protected from the external environment behind the cornea and the eyelid. No subject to deleterious effects of aging, the small-scale radial features of the iris remain stable and fixed from about one year of age throughout life.

1.2 Outline

This paper is divided into five main parts. The *Section 1* introduces what is the position of iris technology in personal authentication. In the *Section 2*, we sum up the state of the art in the domain of iris recognition. The more widely known iris recognition system developed by *J.Daugman* [4] is taken as reference for comparison. The *Section 3* presents in details our approach, and discusses the different issues we chose. The *Section 4* provides test results and illustration of typical iris signature. At last a conclusion is done in *Section 5*, which tasks about the next considerations for the improvement of the proposed solution.

2. Background

The French ophthalmologist *Alphonse Bertillon* seems to be the first to propose the use of iris pattern (color) as a basis for personal identification [3]. In 1981, after reading many scientific reports describing the iris great variation, *Flom* and San Francisco ophthalmologist *Aran Safir* suggested also using the iris as the basis for a biometric. In 1987, they began collaborating with computer scientist *John Daugman* of *Cambridge University* in England to develop iris identification software who published his first promising results in 1992 [4]. Later on a little similar works have been investigated, such as *R.Wildes'* [5], *W.Boles'* [6] and *R.Sanchez-Reillo's* [7] systems, which differ both in the iris features representation (iris signature) and pattern matching algorithms. *R.Wildes'* solution includes (i) a *Hough*

transform for iris localization, (ii) *Laplacian* pyramid (multi-scale decomposition) to represent distinctive spatial characteristics of the human iris, and (iii) modified normalized correlation for matching process. *W.Boles'* prototype operates in building (j) a one-dimensional representation of the gray level profiles of the iris followed by obtaining the wavelet transform zero-crossings of the resulting representation, and (jj) original dissimilarity functions that enable pertinent information selection for efficient matching computation. To finish *J.Daugman's* and *R.Sanchez-Reillo's* systems are implemented exploiting (I) *integro-differential* operators to detect iris inner and outer boundaries, (II) *Gabor* filters to extract unique binary vectors constituting *iriscode*™, and (III) a statistical matcher (logical exclusive OR operator) that analyses basically the average *Hamming* distance between two codes (bit to bit test agreement). Because of unified reference database of iris images does not exist, a classic performance comparison of the described systems is not trivial. However in terms of recognition rates (FAR, FRR), the commercial success of the patented *Daugman's* system speak in his favor. Indeed *Daugman's* mathematical algorithms have been contributing to a commercial solution patented by *IriScan Inc.* This biometric identification platform processes iris recognition through (i) a specific optical unit that enables non-invasive acquisition of iris images, and (ii) a data processing unit. Although capturing a well-defined image of the iris while not interacting actively with the device seems to be one the major challenge we encountered for iris recognition system design, our research focus on the second block both in charge of (j) the enrolment process, and (jj) the matching which quantifies the similitude between two biometric templates.

3. Proposed approach

Our basic experimentation of the *Daugman's* mathematical algorithms for iris processing, derived from the information found in the open literature, led us to suggest a few possible improvements. For justification of these new concepts we implemented in *C* language both the *Daugman's* iris processing unit and our own. Afterwards we tested individually the performances of the different processing blocks previously identified as follows: (1) locating iris in the image, (2) Cartesian to polar reference transform, (3) local features extraction, and (4) matching.

3.1 Locating iris

The first processing step consists in locating the inner and outer boundaries of the iris. In the *Daugman's* system, *Integro-differential* operators (*equation 1*) are used to detect the center and diameter of the iris and the pupil respectively. These operators exploit both the circular geometry of the iris or the pupil. Indeed they behave as a circular edge detector since the sclera is always lighter than then iris, and pupil generally darker than iris for healthy eye.

$$\max(r, x0, y0) = \left\{ \frac{\partial}{\partial r} \int_{0}^{2\Pi} I(r*\cos\theta + x0, r*\sin\theta + y0) \right\} \quad (Eq.1)$$

Where *(x0, y0)* denotes the potential center of the searched circular boundary, and *r* its radius.

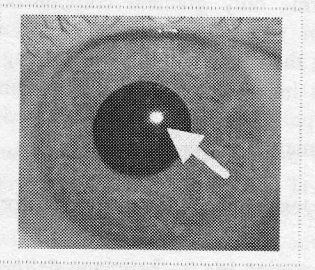

Figure 1: Spot reflection in the pupil.

Using optimized integer code, total computational time for iris detection and localization to single-pixel precision (starting from 640 * 480 image) is about 250 ms [8]. However it appears that *integro-differantial* operators are sensible to the spectacular spot reflection of the non-diffused artificial light (AlGaAS emitting near infrared diodes, which operate in the 750 to 960 nanometers range) pointing toward the center of the user's eye (example in *figure 1*). We used it in order to eliminate artifacts on the eye image due to environmental light. Whenever this spot takes place in the pupil near from the iris/pupil frontier, the detection of the inner boundary of the iris fails.

Consequently we introduce a detection strategy based on the combination of the *integro-differential* operators with a *Hough* Transform. It consists in using firstly an edge calculation technique to approximate the position of the eye in the global image (center of the pupil), and secondly *integro-differential* operators to search more precisely pupil boundary, iris center and iris boundary. Actually the strategy makes use of gradient decomposed *Hough* Transform [11], which is a crafty variant of the *Hough* Transform applied to circular form detection. From the circle equation $(x-x_0)^2+(y-y_0)^2 = r^2$, *r* being the radius, we express the center (x_0,y_0) coordinates in function of the two first-order gradient components (G_x along axe *x*, G_y along axe *y*) as follows:

$$x0 = x \pm \frac{r}{\sqrt{1+\frac{Gy^2}{Gx^2}}}$$
$$y0 = x \pm \frac{r}{\sqrt{1+\frac{Gx^2}{Gy^2}}} \quad (Eq.2)$$

The gradients G_x and G_x are computed both during the unique travel of the eye image. Thus the problem is

reduced to increment the number of occurrences for each supposed center through two accumulators (X_0 in x, Y_0 in y), and to determine the point (x_0,y_0) of the image where it appears a maximum in the accumulators.

$$X_0(x_0) = \sum_x \sum_y \sum_{r=r_{min}}^{r_{max}} nbre.occurences.x_0$$
$$Y_0(y_0) = \sum_x \sum_y \sum_{r=r_{min}}^{r_{max}} nbre.occurences.y_0 \qquad (Eq.3)$$

Considering only gradient components superior to a minimum threshold (defined experimentally) allows reducing the time computation. Taking the sign of the gradients into account plays also an important role to exclude potential center that have coordinates outside of the eye image.

3.2 Cartesian to polar reference transform

Locating iris in the image delineates the circular iris zone of analysis by its own inner and outer boundaries. The *Cartesian to polar reference transform* suggested by *J.Daugman* authorizes equivalent rectangular representation of the zone of interest as shown *figure 2*. In this way we compensate the stretching of the iris texture as the pupil changes in size, and we unfold the frequency information contained in the circular texture in order to facilitate next features extraction. Moreover this new representation of the iris breaks the no-eccentricity of the iris and the pupil. The θ ($\theta \in [0; 2\pi]$) parameter and dimensionless ρ ($\rho \in [0; 1]$) parameter describe the polar coordinate system. Thus the following equations implement $I(x(\rho,\theta), y(\rho,\theta)) \rightarrow I(\rho,\theta)$:

$$\begin{cases} x(\rho,\theta) = (1-\rho) * x_p(\theta) + \rho * x_i(\theta) \\ y(\rho,\theta) = (1-\rho) * y_p(\theta) + \rho * y_i(\theta) \end{cases} \qquad (Eq.4)$$

With:

$$\begin{cases} x_p(\theta) = x_{p0}(\theta) + r_p * \cos(\theta) \\ y_p(\theta) = y_{p0}(\theta) + r_p * \sin(\theta) \end{cases} \qquad (Eq.5)$$

$$\begin{cases} x_i(\theta) = x_{i0}(\theta) + r_i * \cos(\theta) \\ y_i(\theta) = y_{i0}(\theta) + r_i * \sin(\theta) \end{cases} \qquad (Eq.6)$$

Where *rp* and *ri* are respectively the radius of the pupil and the iris, while $(x_p(\theta),y_p(\theta))$ and $(x_i(\theta),y_i(\theta))$ are the coordinates of the pupillary and limbic boundaries in the direction θ.

Figure 2: Iris rectangular representation.

The frontier zones (iris/pupil and iris/sclera) are truncated to avoid noising the iris rectangular representation by other patterns not included in the iris texture: we noticed that (i) the pupil is not perfectly circular, and (ii) the outer iris boundary detection is often not well defined due to the positioning of contact lens bound.

3.3 Local features extraction

The features of the iris are located based on the polar coordinate system. *Gabor's* complex 2D Pass-band filters [9], which offer the best spatial-frequency resolution in the two-dimensional case [10], are proposed by *J.Daugman* to extract textural information of iris images. As a result of the filtering at different frequencies and particular positions in the polar coordinate system, a set of complex values are calculated by convolution. The sign of both the real and imaginary parts of the quadrature image projections from these specific regions of the iris performs a phase quantization of the local texture signal. The time required for computing one complete *iriscode* (256 bytes), once an iris has been located within the image, is about 100 ms. It is important to note that, because of radial correlations between different iris patterns, it exists a dependency within bits extracted in iris codes. The study of the number of degrees-of-freedom indicates in the *Daugman's* system a reduction of the information capacity of the iris code by a factor of 4.05 from 2,048 bits to about 506 bits.

The method discussed in this paper for extraction of local iris features provides a new concept of *instantaneous*-phase and/or *emergent*-frequency, and is related to the work of *J.P.Havlicek* [12] on multi-dimensional *Hilbert* Transform. Although we don't statistically make certain of the improvement of information capacity of the iris code, we will show how *analytic signal*-based approach fulfills most of the desired specifications we need in high confidence iris recognition system.

3.3.1 Instantaneous phase - emergent frequency

The *instantaneous* phase is obtained by constructing the *analytic signal*, which is the combination of the original signal and its *Hilbert* Transform. This *analytic signal* notion of a real one-dimensional signal is introduced by *Gabor* [13] in 1946. For any real signal $x(t)$, we can formulate the complex signal $z_x(t)$ as follows:

$$z_x(t) = x(t) + j.H\{x(t)\} \qquad (Eq.7)$$

Where $H(x(t))$ is the *Hilbert* Transform of $x(t)$. The signal $z_x(t)$ is called *analytic signal*. The *Hilbert* Transform H_x of the real signal $x(t)$ can be expressed in the *Fourier* domain as follows:

$$TF[H_x](f) = (-j.signe(f)).X(f) \qquad (Eq.8)$$

The extension of the *Hilbert* Transform to the multi-dimensional case is not trivial. The particular complex extension of image, called *analytic image*, was introduced by *J.P.Havlicek* [12]. The discrete *Fourier* Transform of the discrete *analytic* image is equal to zero over half of the 2D frequency plane. Over the other half of

the frequency plane, it is equal to twice the discrete *Fourier* Transform of the original real-valued image (except for four frequency samples that are identical to their counterparts in the discrete *Fourier* Transform of the original image). *A.Bovik* [14] gave a practical implementation of the complex extension $z(n_1,n_2)$ of a $N*M$ real-valued image $f(n_1,n_2)$:

$$z(n1,n2)= f(n1,n2)+j.g(n1,n2)= f(n1,n2)+j.H[f(n1,n2)] \quad (Eq.9)$$

In the Fourier domain this reads:

$$G(u,v)= TF[g(n1,n2)] = H(u,v).*F(u,v) \quad (Eq.10)$$

With:

$H(u,v) = -j$ for u=1,2, ... (N/2)-1
$+j$ for u=(N/2)+1, (N/2)+2, ... N-1
$-j$ for u=0, v=1,2, ... (M/2)-1
$-j$ for u=(N/2), v=1,2, ... (M/2)-1
$+j$ for u=0, v=(M/2)+1, (M/2)+2, ... M-1
$+j$ for u=(N/2), v=(M/2)+1, (M/2)+2, ... M-1
0 otherwise

Finally, $z(n_1,n_2)$ is obtained by taking the inverse Fourier Transform of « $Z(u,v) = F(u,v) + j.G(u,v)$ ». A more efficient algorithm for calculating $Z(u,v)$ may be derived by realizing that, for each u and v, $Z(u,v)$ assumes one of only three possible values: zero, $F(u,v)$ *and 2.* $F(u,v)$.

Real-valued image $f(\rho,\theta)$ can be modeled as the following Q multi-component modulation model:

$$f(\rho,\theta) = \sum_{q=1}^{Q} a_q(\rho,\theta).\cos[\varphi(\rho,\theta)] \quad (Eq.11)$$

First of all, to isolate the Q dominant components contained in the texture, we pass the image $f(\rho,\theta)$ through a pass-band filter-bank. The channel responses provide an effective component-wise decomposition using three pass-band filters, which have a one-octave bandwidth. In the frequency domain the 2D real non-dephasor filters are designed by the product of two *Hamming* windows $X_1(u)$ and $X_2(v)$:

$$X(u,v)=X_1(u).X_2(v) \quad (Eq.12)$$

And
$$Xi(f) = \alpha_i + (1-\alpha_i)\cos\pi\frac{f-f_{qi}}{f_{oi}} \quad (Eq.13)$$

Where fq_i is the central frequency of each 1D filter X_i along the frequency axe (u or v). fo_i allows to adjust the -3db bandwidth to one octave in function of fq_i and α_i:

$$f_{0i} = \frac{\Pi}{3.\arccos\left(\frac{1/2-\alpha_i}{1-\alpha_i}\right)} f_{qi} \quad (Eq.14)$$

Then a single-component FM demodulation algorithms [15] is applied directly to the channel responses to identify the FM component modulating functions by using the *analytic image* $z(\rho,\theta)$ as follows:

$$|\Delta\varphi Di(\rho,\theta)| = \arccos\left[\frac{z(\rho,\theta+1)+z(\rho,\theta-1)}{2z(\rho,\theta)}\right] \quad (Eq.15)$$

Any nonzero imaginary component should be discarded prior to the evaluation of the *arccos* function. In our case the frequency demodulation is only focused on the major horizontal information along θ in the rectangular representation of the iris texture. The three different $\Delta\varphi_{Di}(\rho,\theta)$ dominant frequencies form a *emergent* frequency vector. In addition we can of course also extract the instantaneous phase $\varphi_i(\rho,\theta)$ by introducing his algebraic expression as follows:

$$\varphi i(\rho,\theta) = \arctan\frac{\mathrm{Im}(z_i(\rho,\theta))}{\mathrm{Re}(z_i(\rho,\theta))} \quad (Eq.16)$$

Since constructing the analytic image involves the 2D *Hilbert* Transform which is a global Transform, the *instantaneous* phase and the *emergent* frequency depend on the whole signal. The main advantages of using the analytic based technique are that it is computationally efficient: filtering in the *Fourier* domain, pure real filters, and to extract the *instantaneous* phase and/or the *emergent* frequency at each position (ρ,θ) in the iris texture don't need more computation (global Transform).

3.3.2 Generation of the iris code

The coding of the iris features is similar to the *Daugman's* system by thresholding both the module of *emergent frequency* (Eq.15), and the real $\mathrm{Re}(\varphi_i(\rho,\theta))$ and the imaginary $\mathrm{Im}(\varphi_i(\rho,\theta))$ parts of the *instantaneous phase* $\varphi_i(\rho,\theta)$ (Eq.16). Consequently for an $N*M$ real valued rectangular image of the iris texture, nine $N*M$ binary images are available to make the iris code. Nevertheless as eyelid or spot reflection covers some iris areas, the useable field of the iris code is adjusted by truncating small noised zones as shown in *figure 3*.

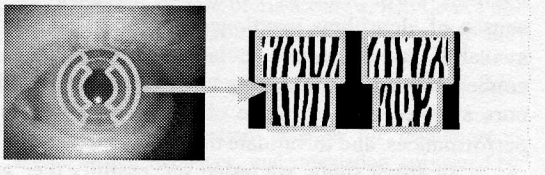

Figure 3: Iris code generation.

3.4 Matching

The final step performs the test *Hamming distance* test, which is generated from the *iriscode* developed for the real-time and from the *iriscode* template from the stored file. In this way, *Hamming distance HD* measures fraction of disagreeing bits resulting from a bit-by-bit comparison of the two codes. In the case of impostor iris-code or randomly generated data, *0.5* is the expected value for *HD*. A criterion, or threshold ($\in$ [0; 0.5]), is chosen and any measured score smaller than this criterion is considered as a rejected identity (impos-

tor), whereas measured score greater than this criterion is considered as a verified identity (authentic). In practice, before the bit-to-bit matching against the iris code in the database, we shift each component of the iris code (binary image) along θ over a range of relative orientations (+/- 7° for example) in order to consider the possible tilt of the head during the eye image acquisition.

4. Experimental results

The *figure 4* gives an illustration of the information representative of the *instantaneous* phase and the *emergent* frequency, extracted from two images of a same iris, acquired a different time (t_0, t_1). As regards of the spectacular similitude between the patterns, the *Tisse et al.* system we described in this paper provides a reliable solution for iris processing.

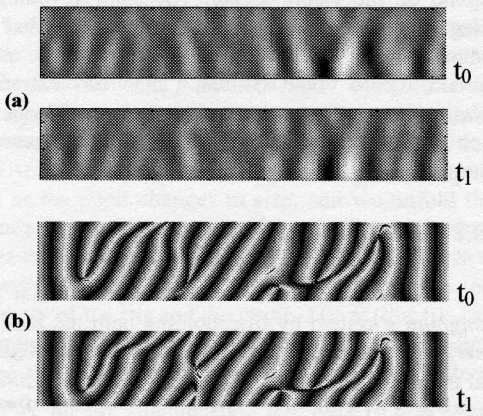

Figure 4: (a) Instantaneous phase function, (b) Emergent frequency function.

The *Tisse et al.* system differs from the *J.Daugman's* system in the following blocks: *locating iris* and *local features extraction*. Because of open source of algorithms mentioned in this article was not available, we developed in language C the different concepts ourself. Comparing *J.Daugman*'s system to ours allowed us to evaluate objectively the respective performances, and to validate the options we chose.

In a first study, we tested successfully the "gradient decomposed *Hough* transform (THGD) / *integro-differential* operators" combination on a database of 50 iris images acquired from 5 cooperatives persons (5 no-blurred images per eye); common range of iris was represented (contact lens, glasses, etc...). It appears that using THGD to localize the center of the eye instead of applying only *integro-differential* operators allows to avoid bad pupil center detection when the spectacular spot takes place near from the frontier between the iris and the pupil (100% of success, against 86% without pre-processing). The computation times are relatively comparable: ≃ 240 ms on PIII-550Mhz.

In a second experimentation, we estimated the False Acceptance Rate (FAR) and the False Reject Rate (FRR) of the *Tisse et al.* iris recognition system. A personal database of more than 300 iris images (10 images captured per eye) was prepared in the *AST* laboratory. The iris codes of size 768 bytes that we compared in this test included a sampling of the binary images resulting of the *emergent frequency* functions. The *figure 5* shows the score distribution observed in function of the two types of population "authentic persons" and "impostors". This FAR and FRR estimation treats only one-to-one verification mode without enrolment. Fixing the criterion of decision to 0.41 implies no false error. Of these attempt, 11% of false reject will be recorded. However, the real FRR will be lower than 3%, because the global reject rate includes the bad localizations (around 8%). A precise analysis of the false localization cases encountered on this database proved that the *integro-differential* operators are not accurate to detect the outer bound of the iris since the eyelashes shade some areas of the texture.

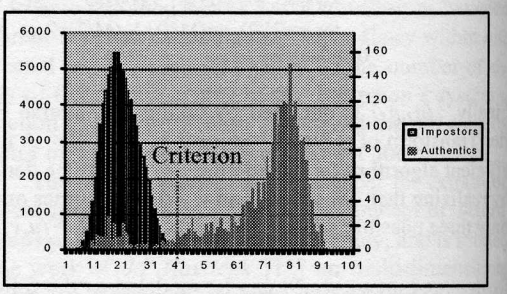

Figure 5: Scores distribution.

Finally the *table1* indicates the time computation consumed by each block of the people identification algorithm using iris recognition that we implemented on a PIII-550Mhz workstation. The average total execution time of a basic verification process doesn't exceed 455 ms, which is suitable for a non-intrusive authentication system.

Table 1: Average time consuming.

	Time consuming	% of total time
Iris localization	250 ms	55
Polar reference	16 ms	3.5
2D Freq. demodulation	187 ms	41
Iris code extraction	< 1 ms	< 0.2
Iris codes matching	< 1 ms	< 0.2
Total time	≃ 455 ms	100

By another way, a third database of 40 iris images was used to confront the "singularity" of the *emergent frequency* with the one of the *local phase*. This database contained only manually pre-localized iris images in order to cancel the influence of inaccurate localization on the performances. In *figure 6*, *Hamming* distances distributions among unrelated iris codes for impostors and pairs of different iris codes for authentics (iris codes of the same size) are reported. We can observe that coding the *emergent frequency* seems to be as pertinent as coding the *local phase*; in the two cases the distribution are clearly well separated, and no overlap occurs.

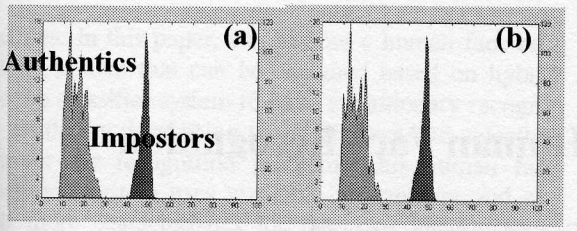

Figure 6: *Hamming* Dist. distribution generated by: (a) *Gabor* filters based *local* phase coder, (b) *Analytic image* based *emergent* frequency coder.

In view of these preliminary evaluations, the *Tisse et al.* system achieves high confidence identity verification based on iris texture using innovative approach. Though the global recognition rates are promising, further efforts should be applied to be insensitive to variations in the conditions of iris images acquisition. In fact we have still to address the design of a specific optical unit (considering illumination, distance from the subject, and focusing problems). In second time it will be also very interesting to study the information capacity of the iris code we used, so that we will be able to look to the best compromise between the iris codes size and the level of security we need in control access.

5. Conclusion

A person authentication technique using human iris recognition is presented, which focus on the image analysis software in charge of the data algorithmic processing. Since recent investigations about iris recognition (*J.Daugman*, *R.Wildes et al.*, *W.Boles*, and *R.Sanchez-Reillo et al.*) didn't look at a unified and free database to provide recognition rates and performances published in the literature, comparing them seems not to be trivial. The *Tisse et al.* approach described in this paper took into account the *J.Daugman's* system as reference, which is the more widely known. The *Tisse et al.* technique suggests alternative solution to *J.Daugman's* mathematical algorithms for local features extraction, which allows adjusting the size of the biometric signature (cf. *iris code*) in function of the desired security level (discrimination problem) without increasing dramatically the computation complexity. This well-suited technique is based on the extraction of *instantaneous* features in the iris texture: the *emergent frequency* and/or *instantaneous phase*. The concept is related to the *analytic image* and *FM demodulation* approaches introduced by *J.Havlicek*. The *Tisse et al.* iris recognition system includes also a robust method for pupil centre detection using a gradient decomposed *Hough* Transform (***T**ransformée de **H**ough suivant les **G**radients **D**écomposés*), which takes advantage of its natural circular shape to improve the success rate of iris localization. In fact, the THGD is used as a first preprocessing stage to enhance the standard iris localization based on *integro-differential* operators. One more time, one must be cautious in the interpretation of the experimental results we obtained because the results presented here are for a small number of iris images. The complete biometric recognition algorithm is successful in verifying the iris patterns. The image analysis software has been implemented in C language with speed maximisation; a standard iris verification processing is executed in $\simeq$ 450 ms. The next step consists in analysing the run-time behaviour and the dynamic memory cost in order to study the portability of the code on future multi-media embedded platform.

6. References

[1] Y.Belganoui, J-C.Guézel and T.Mahé, « La biométrie, sésame absolu ... », Industries et Techniques, France, n°817, July 2000.

[2] M.M.Gifford, D.J. McCartney and C.H.Seal, « Networked biometrics systems: requirements based on iris recognition », BT Technol. Journal, Vol. 17, n°2, April 1999.

[3] A.Bertillon, « la couleur de l'iris », Revue scientifique, France, 1885.

[4] J.Daugman, « High confidence personal identification by rapid video analysis of iris texture », Proc. Of the IEEE, International Carnahan conf. on security technology, 1992.

[5] R.P.Wildes, J.C. Asmuth, G.L. Green and S.C. Hsu, « A system for automated iris recognition », IEEE paper, 1994.

[6] W.W.Boles, « a security system based on human iris identification using wavelet transform », First international conference on knowledge-based intelligent electronic systems, Adelaide, Australia. Ed, 21-23 may 1997.

[7] R.Sanchez-Reillo, C.Sanchez-Avila and J-A.Martin-Pereda, « minimal template size for iris recognition », Proc. BMES/EMBS Conf., IEEE Publication, Atlanta, October 1999.

[8] J.Daugman, «High confidence personal identification by rapid video analysis of iris texture », IEE Conf. Publication n°408, European convention on security and detection, 16-18 May 1995.

[9] D.Gabor, «Theory of communication », Journal IEE, Vol.93, n° III, 1946.

[10] J.Daugman, « Uncertainty relation for resolution in space, spatial frequency, and orientation optimized by two-dimensional visual cortex filters », Journal of optical society of America, Vol. 2, 1985.

[11] D.E.Benn, M.S.Nixon and J.N.Carter, « Robust eye extraction using H.T. », AVBPA'99.

[12] J.P.Havlicek, J.W.Havlicek and A.C.bovik, «the analytic image », IEEE Journal, 1997.

[13] D.Gabor, « Theory of communication », J. inst. Elect. Eng. London, Vol. 93, n° III, 1946.

[14] A.C.Bovik, « The handbook of image processing », Ed. Bovik.

[15] J.P.Havlicek, D.S.Harding, and A.C.Bovik, «Discrete quasi eigenfunction approximation for AM-FM image analysis », Proc. Of the IEEE Int. Conf. on Image Processing, 1996.